Technical Note: Experimental results from a prototype high-field inline MRI-linac

G. P. Liney

Department of Medical Physics, Ingham Institute for Applied Medical Research, Liverpool NSW 2170, Australia; Radiation Physics, Liverpool Cancer Therapy Centre, Liverpool NSW 2170, Australia; School of Medicine, University of New South Wales, Sydney NSW 2170, Australia; and Centre for Medical Radiation Physics, University of Wollongong, NSW 2522, Australia

B. Dong Department of Medical Physics, Ingham Institute for Applied Medical Research, Liverpool NSW 2170, Australia

J. Begg Radiation Physics, Liverpool Cancer Therapy Centre, Liverpool NSW 2170, Australia

P. Vial Radiation Physics & Liverpool Cancer Therapy Centre, Liverpool, NSW 2170, Australia and Radiation Physics Laboratory, Sydney Medical School, University of Sydney, NSW 2006, Australia

K. Zhang Department of Medical Physics, Ingham Institute for Applied Medical Research, Liverpool NSW 2170, Australia

F. Lee Radiation Physics Laboratory, Sydney Medical School, University of Sydney, NSW 2006, Australia

A. Walker and R. Rai Medical Physics, Ingham Institute for Applied Medical Research, Liverpool, NSW 2170, Australia and Radiation Physics, Liverpool Cancer Therapy Centre, Liverpool NSW 2170, Australia

T. Causer and S. J. Alnaghy Centre for Medical Radiation Physics, University of Wollongong, NSW 2522, Australia

B. M. Oborn Centre for Medical Radiation Physics, University of Wollongong, NSW 2522, Australia and Illawarra Cancer Care Centre, Wollongong Hospital, NSW 2500, Australia

L. Holloway Department of Medical Physics, Ingham Institute for Applied Medical Research, Liverpool NSW 2170, Australia; Radiation Physics, Liverpool Cancer Therapy Centre, Liverpool NSW 2170, Australia; School of Medicine, University of New South Wales, Sydney NSW 2170, Australia; Centre for Medical Radiation Physics, University of Wollongong, NSW 2522, Australia; and Radiation Physics Laboratory, Sydney Medical School, University of Sydney, NSW 2006, Australia

P. Metcalfe Centre for Medical Radiation Physics, University of Wollongong, NSW 2522, Australia M. Barton Department of Medical Physics, Ingham Institute for Applied Medical Research, Liverpool NSW 2170, Australia and School of Medicine, University of New South Wales, Sydney NSW 2170, Australia

S. Crozier School of Information Technology & Electrical Engineering, University of Queensland, Brisbane, QLD 4072, Australia

P. Keall Radiation Physics Laboratory, Sydney Medical School, University of Sydney, Sydney NSW 2170, Australia

Corresponding author: Gary Liney gary.liney@sswahs.nsw.gov.au

Abstract

Purpose:

The pursuit of real-time image guided radiotherapy using optimal tissue contrast has seen the development of several hybrid magnetic resonance imaging (MRI)-treatment systems, high field and low field, and inline and perpendicular configurations. As part of a new MRI-linac program, an MRI scanner was integrated with a linear accelerator to enable investigations of a coupled inline MRI-linac system. This work describes results from a prototype experimental system to demonstrate the feasibility of a high field inline MR-linac.

Methods:

The magnet is a 1.5 T MRI system (Sonata, Siemens Healthcare) was located in a purpose built radiofrequency (RF) cage enabling shielding from and close proximity to a linear accelerator with inline (and future perpendicular) orientation. A portable linear accelerator (Linatron, Varian) was installed together with a multileaf collimator (Millennium, Varian) to provide dynamic field collimation and the whole assembly built onto a stainless-steel rail system. A series of MRI-linac experiments was performed to investigate (1) image quality with beam on measured using a macropodine (kangaroo) *ex vivo* phantom; (2) the noise as a function of beam state measured using a 6-channel surface coil array; and (3) electron contamination effects measured using Gafchromic film and an electronic portal imaging device (EPID).

Results:

(1) Image quality was unaffected by the radiation beam with the macropodine phantom image with the beam on being almost identical to the image with the beam off. (2) Noise measured with a surface RF coil produced a 25% elevation of background intensity when the radiation beam was on. (3) Film and EPID measurements demonstrated electron focusing occurring along the centerline of the magnet axis.

Conclusions:

A proof-of-concept high-field MRI-linac has been built and experimentally characterized. This system has allowed us to establish the efficacy of a high field inline MRI-linac and study a number of the technical challenges and solutions.

1. INTRODUCTION

Since the advent of highly conformal intensity-modulated radiation therapy (IMRT), the focus of radiation treatments has shifted from just eradicating the cancer to optimizing margins and improving the therapeutic ratio. Increasingly the advantages of magnetic resonance imaging (MRI) are being incorporated into the planning and monitoring of cancer patients, offering the ability to improve target delineation and the potential for adaptive treatments. A number of groups are pursuing the development of hybrid radiotherapy systems combining an MRI scanner with an external radiation beam delivered from either cobalt sources[1] or a linear accelerator[2–5] to provide real-time MRI-guided treatments. Currently there are four institutions working on integrated systems, each with different approaches, technical challenges, and solutions. There are two main configurations for MRI-linac: inline, where the radiation beam and main magnetic field are aligned and perpendicular, where the radiation beam and main magnetic field are orthogonal to each other. For the inline approach, experimental results have been shown for two low-field iron yoke systems at both 0.2 T (Ref. 3) and a system under development at 0.6 T.[5] In these iron yoke designs, the fringe field is mostly contained within the magnet and so has minimal effect on electron transport (contamination) toward the isocenter.[6] This is in contrast to processes predicted in air-core (non yoke) designs where electrons will be focused toward the beam central axis leading to skin dose increases.[7] The primary advantages however of a higher field (e.g., 1.5 T) are the alignment with standard diagnostic MRI systems and the increased signal-to-noise ratio (SNR) with the

potential for fast imaging for dynamic tracking purposes. This work describes experimental results from a proof-of-concept "phase I" system that was installed as part of a new MRI-linac program. This system, comprising of an exclinical 1.5 T scanner and moveable linear accelerator, has enabled us to examine an inline beam orientation at significantly higher magnetic fields than have previously been used in this geometry. We have investigated and quantified the interactions between the magnetic field and radiation beam as well as the consequences of imaging with the treatment unit in close proximity to the magnet in order to demonstrate the feasibility of a future high field inline system.

2. METHODS

The linear accelerator is a portable unit (Linatron, Varian SIP) capable of producing two photon beams of different energy (nominally 4 and 6 MV) and, respectively, two different maximum dose rates (4 and 8 Gy/min). The unit has been attached to a stainless steel table with a clinical 120-leaf (Millennium, Varian) multileaf collimator (MLC) in front to provide dynamic field collimation. The whole system is mounted on a sliding rail and brake system with the advantage of permitting a change in the source to isocenter distance (SID) from 1.9 to 3.3 m. The magnet is a 1.5 T scanner (Siemens Sonata) operating with 40 mT/m and 200 (mT/m)/s gradients, eight independent radiofrequency (RF) channels, and a 60 cm bore diameter. In order to match the beam line height, the magnet was raised on blocks and positioned 40 cm from a specifically designed RF cage wall. The cage is designed with a recess and removable RF hatch that allows access to the magnet (for maintenance). In normal operation, the panel, comprising of 1 mm copper and 10 mm wood, is *in situ* and the beam traverses through it. The magnet was passively shimmed with the treatment unit in the closest position (SID = 1.9 m). Verification of image-beam congruence was made using a dedicated phantom (Leeds Test objects, UK). Figure 1(a) shows a photograph of the MRI-linac prototype and a schematic diagram of the experimental setup is shown in Fig. 1(b).

The following series of experiments was performed to investigate the effects and mutual interactions of operating an inline MRI-linac.

2.A. Beam-on image quality

The first beam-on image acquired on December 24th, 2015 was of an *ex vivo* macropodine (kangaroo) phantom using the integrated body RF coil and a nominal 3 Gy irradiation using a 3 × 3 cm field at isocenter and 2.8 m SID. An attempt was made to reduce radiation induced effects by delivering a small field through the large diameter RF coil that resides permanently inside the magnet bore. Imaging was acquired both with and without the beam turned on during the acquisition of a T_1-weighted spin-echo (TE/TR = 14/620 ms) sequence. Subsequently a bottle containing doped water was imaged with a 6 channel surface coil array and set up deliberately to position the coil in the path of the beam using the same field size. Images were acquired in both a static and dynamic manner with the latter using a T_1-weighted TrueFISP (TE/TR = 2.2/4.4 ms) sequence to examine the temporal relationship with beam state. A total of 200 dynamic images were acquired with the following changes in operation: (images 1–50) beam off with MLC closed; (51–100) beam on with MLC closed; (101–150) beam on with MLC fully retracted; and (151–200) beam off. The percentage signal change was measured in regions placed within the phantom and background noise. The static beam-on and beam-off image test was performed on a daily basis for a period of three weeks as part of the daily QA of the system.

2.B. Proximity of treatment unit on field uniformity

In addition to passive shimming, a system "tune-up" shim was performed with the Linatron at each table position with both linear (gradient offset) and higher order (shim current adjustment) settings recorded. Two gradient echo images (TE = 10 and 12 ms) were acquired in a 25 cm diameter doped-water sphere and a phase difference map reconstructed to visualize the changes in the B_0 field with the treatment unit at each table position both with and without adjusting shim settings. This variation was further quantified in terms of geometric accuracy using a previously described large field-of-view (FOV) test object[8] which enabled the distortion over a 40 × 40 × 38 cm volume of interest to be examined with changes in shim settings.

2.C. Dosimetry in magnetic field

For preliminary assessment of the electron contamination focusing effect, a series of Gafchromic (EBT3) films were positioned in air at nine locations along the beam trajectory [see Fig. 1(b): cage wall, magnet entrance, within bore and exit]. Percentage depth dose (PDD) measurements were also performed using an open photon field and film placed in solid water parallel to the beam direction, with the surface of the solid water at the isocenter. Film was digitized using an EPSON Perfection V700 scanner, calibrated via Radiochromic.com[9] and analyzed in ImageJ. These measurements were repeated using the same setup with the magnet ramped down prior to the scanner being removed, in order to provide a zero magnetic field comparison. Electron contamination due to focusing in the magnetic field was additionally measured along the central axis by delivering 3×3 cm^2 fields at 4 cm off axis. Photon fields were delivered to both solid water and solid lung material.

A final set of experiments were performed using a standard electronic portal imaging device (EPID) (Perkin Elmer x-ray panel) which was positioned at the rear of the magnet to assess the feasibility of using this equipment in the high fringe field. Standard contrast-to-noise ratio (CNR) and resolution [modulation transfer function (MTF) at f_{50} and f_{30}] measurements were made using the QC-3 phantom (Standard Imaging, USA). Additionally, measurements of SNR in the MRI images were made with the EPID in operation. The EPID, which had the cover and the electron build-up layer (1 mm copper) removed in order to image the electron contamination distribution, was also irradiated with 2×7 cm field which was incrementally shifted in the lateral direction to further investigate the characteristics of the electron contamination focusing effect.

3. RESULTS

3.A. Beam-on image quality

Figure 2(a) shows the first beam-on image and the repeat image without irradiation. There was negligible difference between these two images with values of mean ± SD (signal background) equal to 503 ± 16 and 501 ± 17 with beam on and off, respectively.

However, using the surface coil arrangement in the path of the beam, an elevation of background signal of up to 24% was observed with a negligible change in phantom signal. Although not easily discernible in the images with conventional window settings, an interference pattern was clearly evident when the raw (*k*-space) data were examined. This interference pattern was shown to be synchronous with the beam and was reduced in intensity at a lower trigger (dose) rate. Figure 2(b) plots the background signal measured in the dynamic image sequence. This shows a large change in signal with beam on which is not present when the linear accelerator is operating but with the MLC closed. Repeat experiments over 21 days (using a low dose rate) showed the ratio of beam on/off signal in the phantom and background region to be 1.01 ± 0.01 and 1.08 ± 0.01, respectively.

3.B. Proximity of treatment unit on field uniformity

Figure 3 shows phase difference maps which are proportional to changes in field uniformity (ΔB_0). As the treatment unit is moved closer to the magnet, there is significant disturbance in the field at the magnet isocenter as shown by the increasing nonuniformity and range of colors displayed in these images. When dynamic shimming was employed for each table position, this loss of uniformity was recovered in each case. Results with the large FOV distortion phantom demonstrated that only 22% of the imaged volume exhibited distortion of less than 2 mm (maximum 8.9 mm) when no reshimming was carried out to compensate changing SID from 2.8 to 1.9 m. These figures improved to 97% (and a 2.5 mm maximum value) and 100% (0.9 mm maximum), with linear adjustment and full high order adjustments, respectively.

3.C. Dosimetry in magnetic field

Figure 4 (left) shows an example of the irradiated film located perpendicular to the beam at 62 cm from the isocenter in the target direction [position number 3 in Fig. 1(b)]. In addition to the primary field (7.5 cm square), there is a central hypointense (hotspot) region of approximately 2.5 cm in size arising from the focusing of electron contamination back towards the beams central axis. This was observed on all films apart from at the cage wall; the area of focus appeared to approach a minimum in size at the isocenter (1.5 cm area in a 9 cm primary collimation) and then increases in size upon exit from the magnet bore as the magnetic field

rapidly reverses direction from high to low. These two regions became indistinct at the furthest film positions. The EPID device was also successfully used to show this effect at the rear of the magnet [Fig. 4 (right)]. The signal intensity ratio between the hyperintensity at center and edge of the field was 1.8. Increasing the offset of the primary field away from the central axis was noted to separate these two radiation components. The offset x-ray beam is shown while the electron contamination distribution remains deposited along the magnet isocenter. The ratio of signal between these two distinct regions at a 7.5 cm field offset was equal to 1.3.

More generally, the fringe field (up to 800 G) had no impact on the function or imaging performance of the EPID as determined by standard metrics. Values of MTF (f_{30} = 0.82 and f_{50} = 0.57) and CNR = 665 were well within normal expected values for clinical linear accelerators. However, MR images acquired with the EPID turned on exhibited a severe reduction in SNR from 82 to 3. This value increased to 12 with careful shielding of power cables wrapped in aluminium foil and remedied completely by use of an alternate power supply. Moderate RF artifacts were also noted and the source of these was identified as being from the data connection cable.

Figure 5(a) shows an example of depth dose measurements acquired with an open field in solid water comparing the difference with and without magnetic field present (normalized at 5 cm). This plot demonstrates an increase in surface dose of up to 300% due to the electron focusing effect from the in-line magnetic field with the dose returning to baseline values at 1.6 cm. Figure 5(b) compares digitized film results with the field shifted laterally to visualize the primary and secondary contributions of dose separately in both solid water and lung equivalent materials. The smaller electron density of the lung material demonstrates the electron contribution to a greater depth.

4. CONCLUSIONS

A prototype system has been built which has allowed us to establish the feasibility of a high field MRI-linac in the inline beam orientation. This proof-of-concept system has allowed us to study a number of the technical challenges and quantify its operating characteristics. Image quality has been shown to be unaffected by the beam whereas interference has been demonstrated using a specific RF coil setup where the beam deliberately traverses the coil. This is in contrast to previous studies which have either shown no observable effect[10] or described a reduction in SNR attributed as being caused by induction in the copper conductor directly.[11] Our results show a large increase in background intensity, which does not occur when the linear accelerator is in operation and the MLC is closed, thereby showing that it is not extraneous noise from the accelerator (which is outside a RF cage). The elevation of noise has the potential to reduce overall SNR within the image but this is highly dependent on the RF coil setup. In fact the effect could be used advantageously; for example, a combination of RF coil elements could be positioned in such a way so that one receives the radiation beam in the manner described above but is far enough away from a second element that is sensitive to the imaged object alone. Further work will explore the potential of this approach for real-time beam monitoring.

The effectiveness of a linear gradient offset (predominantly in the *z*-gradient) to mitigate field nonuniformity caused by the proximity of the treatment has also been shown over a range of SID. This is important as our second prototype—unlike clinical scanners—will not have high order dynamic shim coils. Current experience also suggests that EPIDs (to be used predominately for dosimetry) will be relatively easily incorporated into our final MRI-linac system with a few minor filter panel modifications. Radiation measurements in film and EPID have revealed the focusing of secondary electron contamination into the center of the primary field that has only previously been modeled[7] or described for substantially higher fields.[12] These electrons have been shown to be easily attenuated and could be removed (for example) by the patient device we are proposing.[4] Intrapatient secondary electron focusing may hold advantages when compared to the dosimetry of perpendicular orientated systems.[13] As the electron will traverse longitudinally, it is logical to expect the lateral range to be reduced. In low density medium such as lung, the penumbral flaring that occurs due to electron disequilibrium will be reduced by the forward focusing. While there is no simple quantification of this effect, it is significant enough to have an impact on target coverage and has been shown using Monte Carlo methods to provide a significant dose enhancement effect[14] which warrants further investigation. In future work, we will replace the 1.5 T

magnet with a specially designed 1.0 T split bore magnet to allow the construction of a fully integrated second prototype and extend these preliminary findings.

References

1 J. F. Dempsey et al., "A device for real time 3D image-guided IMRT," Int. J. Radiat. Oncol., Biol., Phys. 63, S202 (2005).

2 J. J. W. Lagendijk, B. W. Raaymakers, and A. J. E. Raaijmakers, "MRI/linac integration," Radiother. Oncol. 86, 25–29 (2008).

3 B. G. Fallone et al., "First MR images obtained during megavoltage photon irradiation from a prototype integrated linac-MR system," Med. Phys. 36, 2084–2088 (2009).

4 P. J. Keall, M. Barton, and S. Crozier, "The Australian magnetic resonance imaging-linac program," Semin. Radiat. Oncol. 24, 203–205 (2014).

5 B. G. Fallone, "The rotating biplanar linac-magnetic resonance imaging system," Semin. Radiat. Oncol. 24, 200–202 (2014).

6 A. Keyvanloo, B. Burke, J. St. Aubin, D. Baillie, K. Wachowicz, B. Warkentin, S. Steciw, and B. G. Fallone, "Minimal skin dose increase in longitudinal rotating biplanar linacMR systems: Examination of radiation energy and flattening filter design," Phys. Med. Biol. 61, 3527–3539 (2016).

7 B. M. Oborn, P. E. Metcalfe, M. J. Butson, A. B. Rosenfeld, and P. J. Keall, "Electron contamination modelling and skin dose in 6 MV longitudinal field MRIgRT: Impact of the MRI and MRI fringe field," Med. Phys. 39, 874–890 (2012).

8 A. Walker, G. P. Liney, L. Holloway, J. Dowling, D. Rivest-Henault, and P. Metcalfe, "Continuous table acquisition MRI for radiotherapy treatment planning: Distortion assessment with a new extended 3D volumetric phantom," Med. Phys. 42, 1982–1991 (2015).

9 I. Mendez, V. Hartman, R. Hudej, A. Strojnik, and B. Casar, "Gafchroimic EBT2 film dosimetry in reflection mode with a novel plan-based calibration method," Med. Phys. 40, 011720 (9pp.) (2013).

10 S. J. Hoogcarspel, S. P. M. Crijns, J. J. W. Lagendijk, M. Van Vulpen, and B. W. Raaymakers, "The feasibility of using a conventional flexible RF coil for an online MR-guided radiotherapy treatment," Phys. Med. Biol. 58, 1925–1932 (2013).

11 B. Burke, K. Wachowicz, and B. G. Fallone, "Effect of radiation induced current on the quality of MR images in an integrated linac-MR system," Med. Phys. 39(10), 6139–6147 (2012).

12 A. F. Bielajew, "The effect of strong longitudinal magnetic fields on dose deposition from electron and photon beams," Med. Phys. 20, 1171–1179 (1993).

13 A. J. E. Raaijmakers, B. W. Raaymakers, and J. J. W. Lagendijk, "Integrating a MRI scanner with a 6 MV radiotherapy linear accelerator: Dose increase at tissue-air interfaces in a lateral magnetic field due to returning electrons," Phys. Med. Biol. 50, 1363–1376 (2005).

14 B. M. Oborn, Y. Ge, N. Hardcastle, P. E. Metcalfe, and P. J. Keall, "Dose enhancement in radiotherapy of small lung tumors using inline magnetic fields: A Monte Carlo based planning study," Med. Phys. 43, 368–377 (2016).

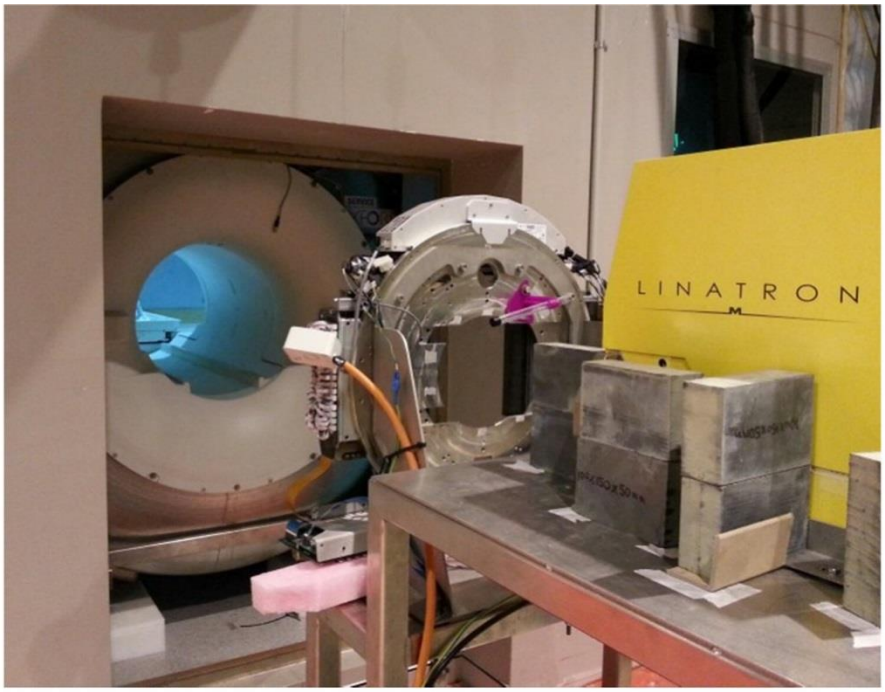

(a)

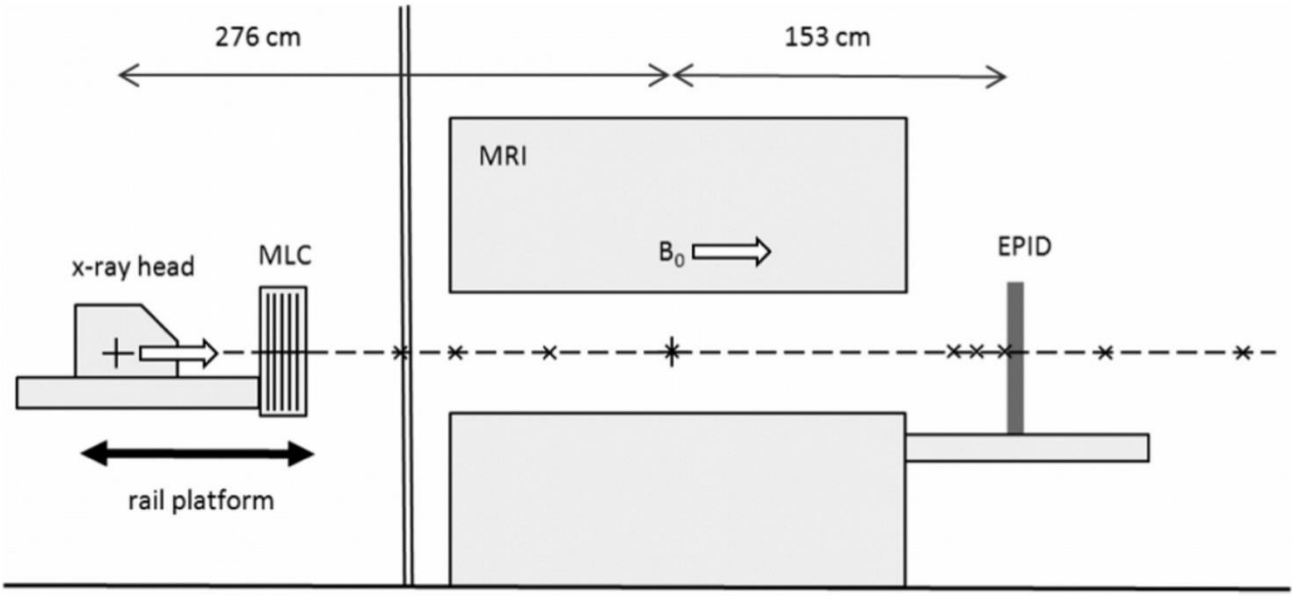

(b)

Figure 1. (a) A photograph showing the prototype system with the treatment unit at the middle rail position. The recess in the RF cage wall allows the linear accelerator to be positioned in close proximity to the magnet (RF panel has been removed). Lead shielding can also be seen around the x-ray head to reduce leakage and back scattered dose. (b) Schematic diagram showing the layout of the linear accelerator and MRI scanner with SID = 2.76 m. Crosses indicate the relative positions of the (9) film measurements.

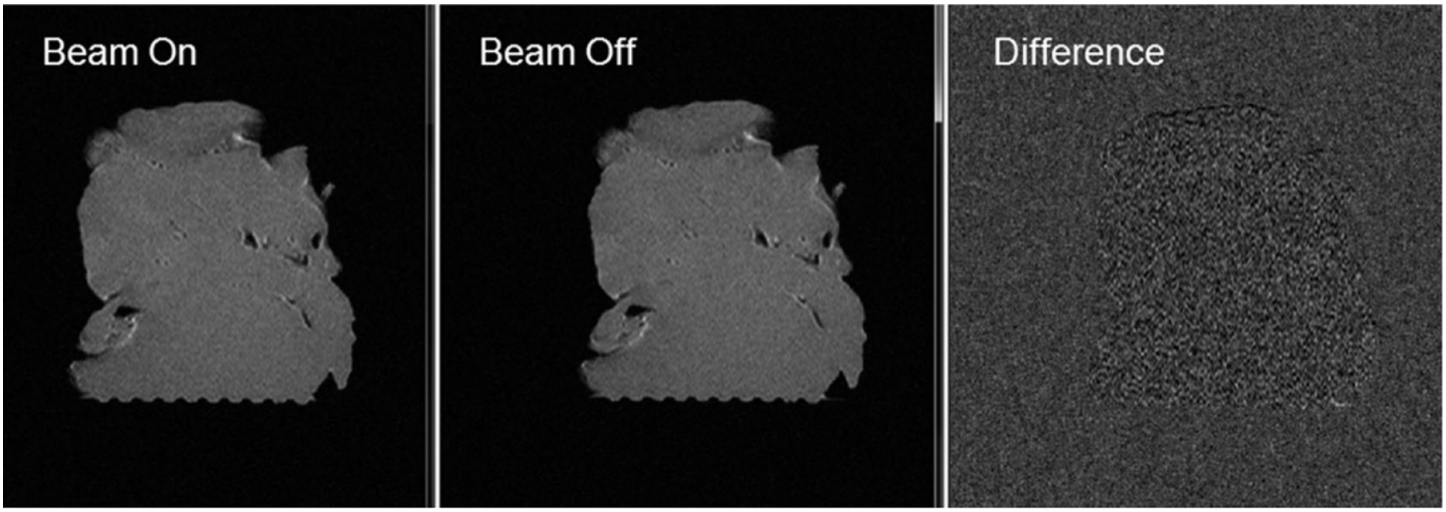

(a)

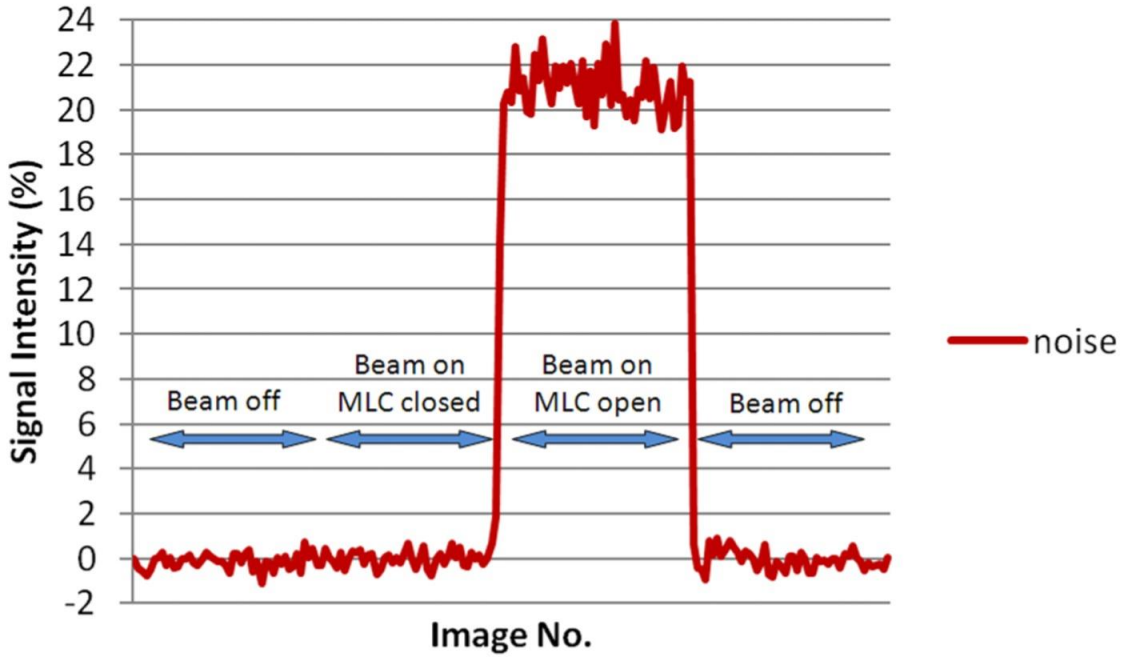

(b)

Figure 2. (a) Image of *ex vivo* kangaroo phantom with (left) beam on (SNR = 31), (center) repeated with beam off (SNR = 30), and (right) subtraction of the two images showing a negligible difference. (b) A plot of percentage change in background intensity versus image number from a series of dynamic scans in which the beam is first off, then turned on with MLCs closed, MLCs then fully retracted while the beam is on, and finally the beam is turned off. Up to 24% increase in background signal change is seen from the interaction between the beam and the RF coil.

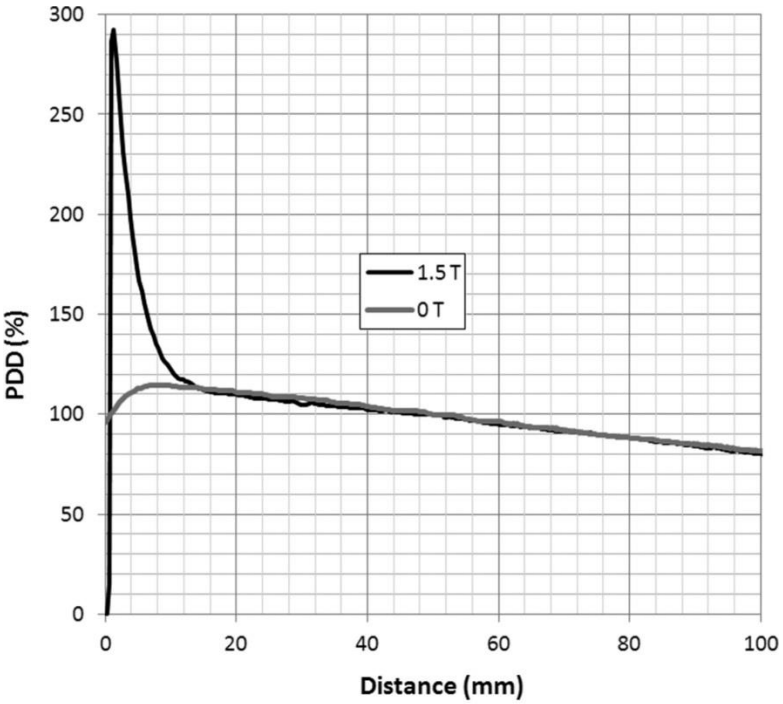

(a)

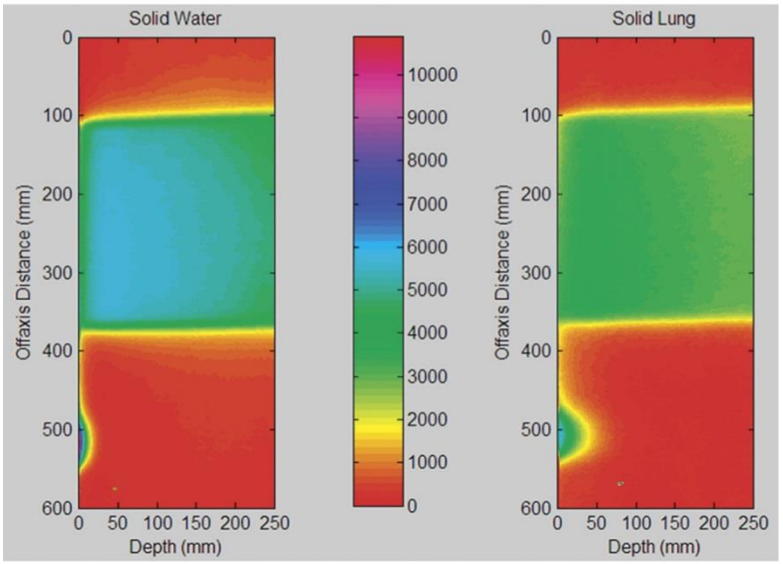

(b)

Figure 3. Phase difference maps acquired in a 25 cm diameter spherical water phantom. Images are at isocenter with the Linatron at SID shown, first without shimming (top row) and then with table-position shim adjustment (bottom row). Images on the top row show increasing nonuniformity as B_0 is disturbed by the treatment unit moving closer to the magnet. Each image on the bottom row is qualitatively similar to the baseline image at 2.8 m.

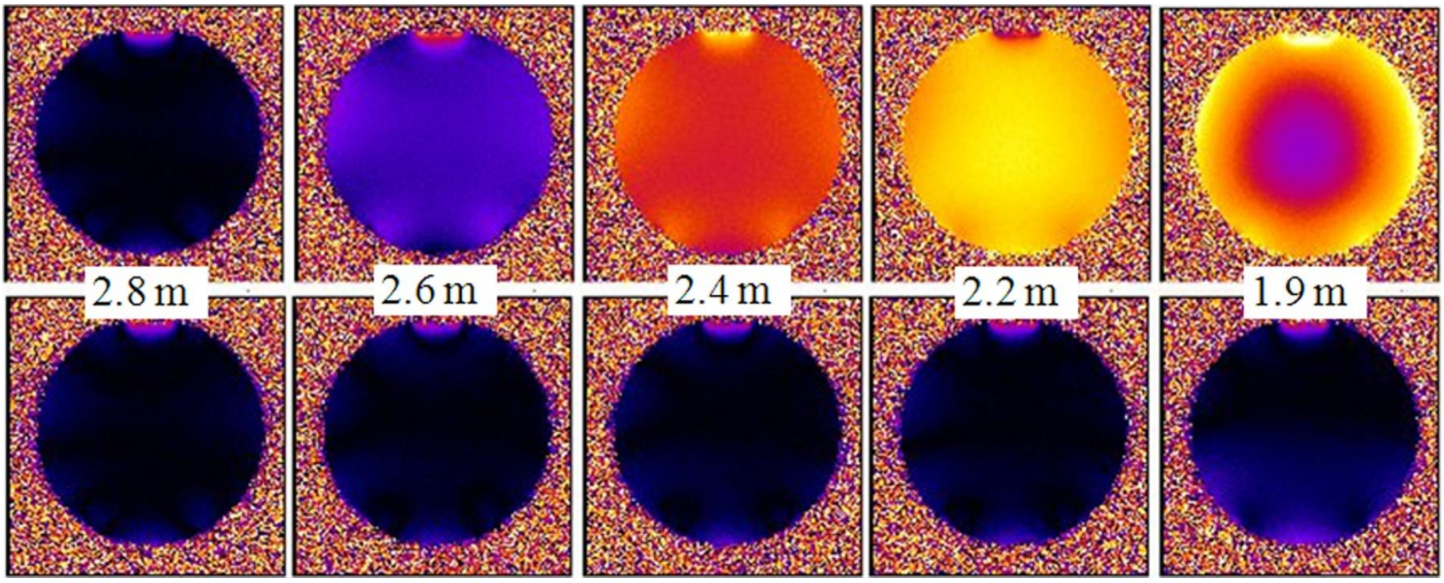

Figure 4. (left) A piece of Gafchromic (EBT3) film positioned 62 cm from the magnet isocenter illustrates electron focusing in the center of the primary field. (right) Electronic portal images acquired with the panel outside the bore and irradiated with a rectangular field on axis and repeated with the primary collimation set 7.5 cm off-axis.

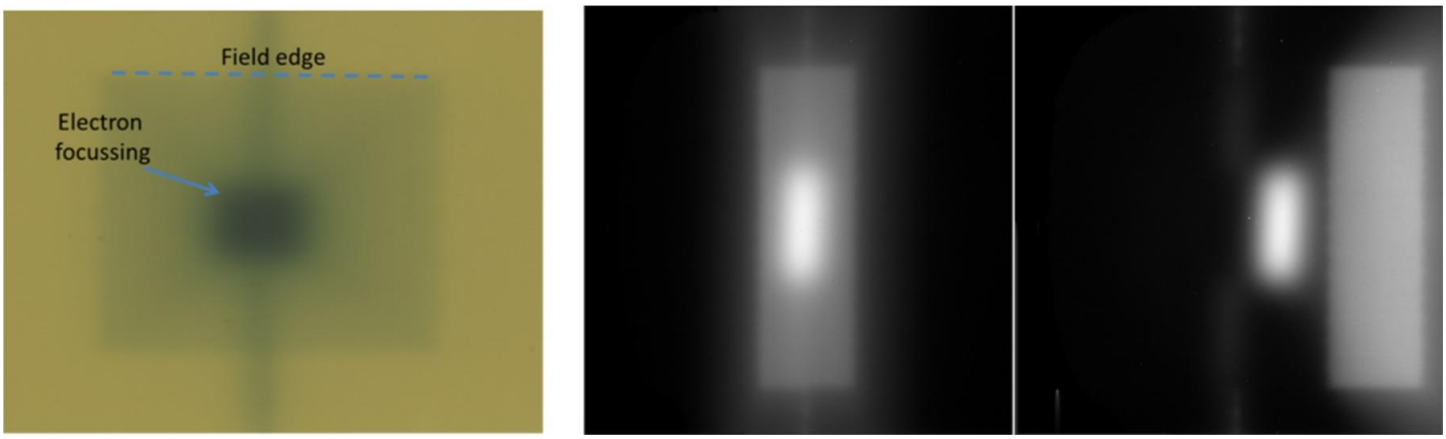

Figure 5. (a) Percentage depth dose measured from calibrated film in solid water in both zero magnetic field and 1.5 T in-line magnetic field. (b) Digitized and calibrated pieces of film taken in (left) solid water and (right) lung equivalent material using an off-center square field to demonstrate the depth dose separately from photon and electron components.